http://dx.doi.org/10.17159/2411-9717/2015/v115n8a16

Investigation into strata behaviour and fractured zone height in a high-seam longwall coal mine

by G. Song* and S. Yang*

Synopsis

The development of techniques and equipment for single-pass high-seam longwall mining in China is reviewed. Some methods used to obtain the fractured zone height are discussed. The boundary between the caved and fractured zones is generally not clear, but one important difference that distinguishes the two zones is that horizontal compressional forces exist only between blocks of fractured zone. Based on this, a theoretical method is presented to investigate the destabilizing modes of the main roof (by sliding or rotation) and is used to determine if the main roof is in the caved or fractured zone. This method considers the mining height, immediate roof thickness, bulking factor, main roof thickness, main roof strength, main roof periodic weighting interval, and vertical stress in the overlying strata. To verify the method, a representative physical model of Wangzhuang coal mine is developed. The movement of overlying strata and fractured zone height are thus obtained. According to the results, the total collapsed height of the strata reaches about 70 m above the coal floor; the first main roof bending interval is 45 m and periodic bending distance is 10–15 m; the maximum strata subsidence is around 62 mm; and the presence of a three-hinged arch causes the fluctuation of subsidence in the same stratum level. Based on the theoretical and experimental analysis, the middle of the main roof is considered the boundary between caved and fractured zone; the caved and fractured zone heights are about 21 and 49 m respectively.

Keywords

thick coal seam, single-pass longwall mining, physical modelling, bulking factor, caved zone, fractured zone, roof strata behaviour.

Introduction and background

Thick coal seam mining in China

Thick coal seams (>3.5 m) account for about 44% of the coal rescource/reserves and more than 40% of the total annual production in China (Zhao 2004; Wang 2009). Three mining methods – slice mining, top coal caving, and single-pass high-seam longwall mining – are frequently used in underground thick-seam operations. Compared with slice mining and top coal caving, high-seam single-pass longwall mining significantly simplifies the mining processes, reduces roadway excavation, and improves coal production, productivity, and recovery. The favourable economics, high production, and technical simplicity make high-seam single-pass longwall mining one of the most popular underground mining methods for thick coal seams in China.

Highly mechanized mining equipment for longwall faces was first introduced to China in 1978. However, preliminary trials were not successful due to equipment capacity limits and roof control problems. The next few decades, however, witnessed great progress in coal production, mining heights, and panel widths, which were due to improvements in mining techniques and equipment, especially the hydraulic-powered shield (Wang, 2013). The maximum annual production in a single panel stood at less than 2.5 Mt in 1998, but this increased dramatically to 12 Mt in 2008 and 14 Mt in 2011 (Yuan *et al.*, 2010). In 2007, Shangwan coal mine developed the world's first 6.3 m single-pass high-seam longwall face. The mining height increased to 7 m in Bulianta mine in 2009. The trend of increasing shield maximum support height from 2000–2014 is shown in Figure 1, and Figure 2 shows the shield used in Wangzhuang mine. Table I lists the parameters of the panels and equipment, which compares the improvement of these faces from 6.3 m to 7 m. The increase of mining height has led to nearly 10% improvement in recovery and around 1.2 Mt of additional annual production, but requires heavier and larger installed-power equipment.

Physical modelling investigation

The fractured zone height and roof control are the most important issues in single-pass high-seam longwall mining in China. It is believed that strata movement is likely to be more severe; face failure and roof falls more frequent (Yuan *et al.*, 2010), and the caved/fractured zone height higher due to larger mining thickness and high-intensity mining activity (Sun *et al.*, 2013). Generally, physical modelling is used to study the dynamic movement process in overlying strata during mining. This model can record the roof

* *College of Resources and Safety Engineering, China University of Mining and Technology, Beijing, China.*

 ISSN 2225-6253. Paper received May 2015 and revised paper received June 2015.

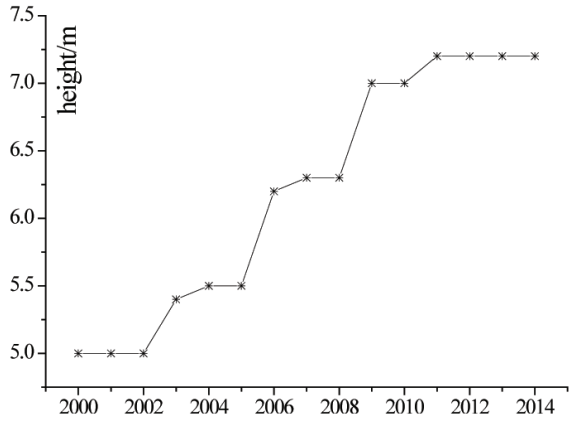

Figure 1 – Maximum height of shield from 2000

Figure 2 – Type ZY15000/33/72D shield used at Wangzhuang

failure development, strata subsidence, and the structure of roof blocks. Li *et al.* (2005) compared the results of numerical and experimental studies of strata movement above the collapsed gob and suggested that experimental research can be used to verify numerical findings. Yang *et al.* (2009) investigated the influence of mining thickness on abutment pressure and three zones (caved zone, fractured zone, and continuous subsidence zone over goaf) in a physical model experiment. The results showed that the area influencd by abutment pressure and the height of the caved/fractured zone increase as mining height increases. The floor movement can also be observed in physical simulation experiments. Jiang *et al.* (2011) studied the failure of coal seam floors above confined water experimentally and analytically. The displacement of floors was recorded, indicating that the floors move upwards and the displacement increases as the face advances. Three zones in the floors (mining-induced fissure zone, water-resisting zone, and confined water ascending zone) were observed. Zhao *et al.* (2013) developed this study further by applying horizontal loads to the experimental model according to the ground stress survey. They concluded that the largest upward movement occurs 30 m behind the panel, and the closer the floor is to the aquifer, the larger the displacement would be.

Panel 8101 at Wangzhuang is the first high single-pass longwall face in this mine, with no previous strata behaviour data available. Thus obtaining this data is of great significance for better control of the roof and for successful mining. A theoretical analysis and a physical model to obtain the height of caved/fractured zone and Wangzhuang and describe roof movement behaviour are presented in this paper.

Theoretical analysis of caved, fractured zone, and strata behaviour

Previous work

Strata movement and ground subsidence have been investigated in detail by researchers around the world. Wagner *et al.* (1991) reviewed the ground subsidence at South African collieries during total-seam underground extraction. The vertical subsidence in South African mines was found to be less than at European mines, due to the presence of competent layers in the overlying strata. Singh *et al.* (1999) monitored strata parameters and the behaviour of

Table I

Comparison of 6.3 m and 7.0 m panels

Colliery	Shangwan	Bulianta	Bulianta	Shangwan
Panel built (year)	2007	2007	2009	2010
Panel number	51202	32301	22303	12205
Panel height, m	6.3	6.3	7.0	7.0
Panel width, m	301	300	301	319
Panel length, m	4466	5220	4966	4231
Recovery	87.1%	88.7%	96.7%	Around 97%
Production, Mt	10.87	Around 11	Around 12	Around 12
Shield type	ZY10800/28/63	ZY10800/28/63	ZY18000/32/70	ZY18000/32/70
Shield load density, MPa	1.05-1.12	1.05-1.12	1.39-1.43	1.39-1.43
Shield total weight, t	45	45	69	69
Shearer type	SL1000	SL1000	SL1000 (7 m)	SL1000 (7 m)
Shearer mining range, m	2.5-6.2	2.5-6.2	2.7-7	2.7-7
Shearer total installed power, kW	2×1080	2×1080	2590	2590
Shearer total weight, t	135	135	110-155	110-155
Conveyor type	48 mm AFC%	48 mm AFC%	PF6H-1542	PF6H-1542
Conveyor total installed power, kW	3×1000	3×1000	3×1600	3×1600
Conveyor carrying capability, t/h	—	—	6000	6000

powered support for exploitation of a 7.5 m sublevel caving face in India through field observation. The movement of roof strata was visualized in a simulated physical model. Cui *et al.* (2000) used nonlinear geometric field theory to predict the surface subsidence induced by underground mining. Ju *et al.* (2013) investigated the structural characteristics and behaviour of key/competent strata in the overburden of a 7 m high panel through *in-situ* observation and a laboratory physical model.

Generally, the collapsed strata above the goaf can be classified into three zones; the caved zone, fractured zone, and continuous subsidence zone (Qian and Shi, 2003). It is important to know the fractured zone height and boundaries of these zones, especially for mines with roof water inrush potential. Immense amounts of field monitoring work have been conducted in China, and empirical equations to calcalate fractured zone height have been derived, shown as Equations [1] and [2] (State Bureau of Coal Industry, 2000).

$$H_c = \frac{100\sum M}{4.7\sum M + 19} \pm 2.2 \quad [1]$$

$$H_f = \frac{100\sum M}{1.6\sum M + 3.6} \pm 5.6 \quad [2]$$

Based on empirical equations, the heights of the caved and fractured zone at Wangzhuang mine are 10.8–15.2 m and 40.5–51.6 m, respectively.

Since then, many investigators have carefully reviewed and expanded the research on fractured zone height. Xu (2009, 2012) and Wang (2013) believed that the position of the key stratum is closely related to fractured zone height. Hu (2012) developed the factors influencing fractured zone height (incorporating mining height, strata, panel length, seam depth, and panel advancing speed) and obtained a formula using multiple regression analysis to calculate fractured zone height. Kang (2009), Wu (2012), and Sun (2013) measured the fractured zone height using different methods such as borehole camera, drilling fluid, and drilling resistivity.

Theoretical solution

To obtain a specific height of the caved and fractured zones, it is necessary to clearly identify the boundary of these two zones. In general, the immediate roof is essentially soft and weak mudstone, which caves in after the shields are advanced; whereas the main roof – the massive, thick, and strong roof above the immediate roof – will bend, sag, split, rotate, or detach after a considerable distance of overhang for a long period (Das, 1999; Qian, 2003). The breakage modes of the main roof include rotation and sliding. The broken main roof blocks could be assigned to the caved or the fractured zone, depending on the horizontal compressional force between broken roof blocks. If rotation occurs in the main roof, it is likely that a horizonal compressional force is generated between roof blocks and this main roof is thus incorporated in the fractured zone. On the other hand, the main roof is included in the caved zone if sliding is seen, implying that no compressional force was exerted. Figure 3(a-c) shows the rotation and sliding of the main roof during first and periodic weighting. Figure 3d shows the three-hinged arch formed in a rotation of the main roof.

The breakage style of the main roof thus determines whether the main roof is assigned to the caved or the fractured zone. Hou (2003) believed that if h>1.5·Δ(where h is main roof thickness, and Δ is the void between caved immediate roof rock mass and overhang main roof), then the main roof is included in the fractured zone. Obviously, the void between caved immediate roof and overhang main roof is closely related to main roof breakage. In the case of a smaller void (Figure 3b), rotation is more likely to occur due to the support of waste rock on the floor before main roof blocks detach completely. A larger void is more likely to lead to main roof sliding. The main roof is then classified in the caved zone, with no compressive force formed between roof blocks (Figure 3c).

Bulking factor (K_ρ), the ratio of broken rock bulk to original rock bulk, is used to describe the property of the rock mass (see Equation [3]). Das (2000) believed that the bulking factor controls the ground subidence. He classified superincumbent strata over a longwall panel into caving zone, unfilled void, freely detached zone, weighting zone, and stable superincumbent roof zone, and demonstrated that 45–60% of the total caving height is filled with bulk volume, leaving the remaining 40–55% as unfilled void that causes subsidence through:

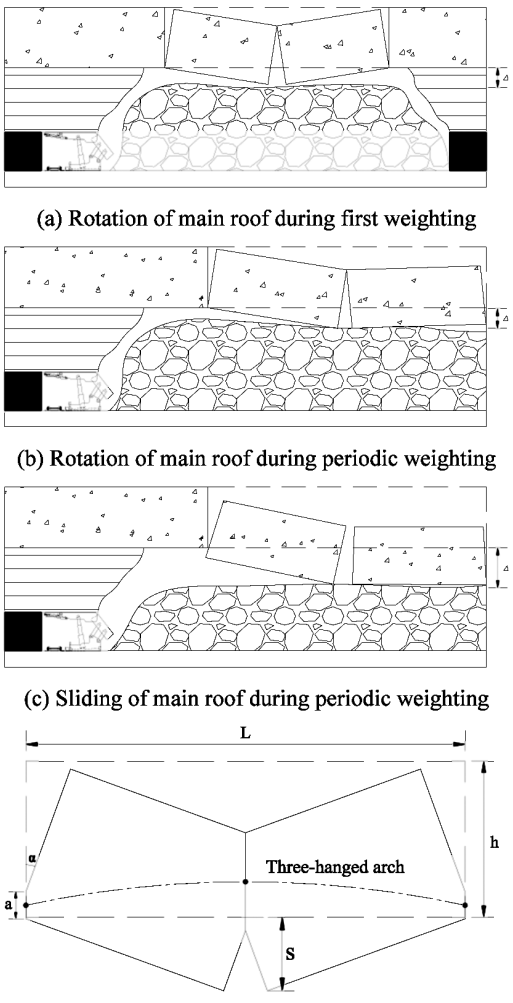

(a) Rotation of main roof during first weighting

(b) Rotation of main roof during periodic weighting

(c) Sliding of main roof during periodic weighting

(d) Three-hinged arch in main roof rotation,

where h is main roof thickness; s is main roof sinkage; α is angle of rotation; L is main roof weighting interval; a is length of blocks contact surface.

Figure 3 – Main roof breakage styles

$$K_\rho = \frac{v_1}{v_0} \quad [3]$$

where v_0 is the original bulk of rock, and v_1 is the bulk of the collapsed rock mass.

During mining, the weak immediate roof caves in and the broken rock is randomly deposited on the floor. Equation [4] applies if the collapsed immediate roof rock mass completely fills the gob. In this case, no void is left.

$$M + \sum h = K_\rho \sum h \quad [4]$$

where M and $\sum h$ are the mining height and roof thickness before collapse, respectively.

Otherwise, unfilled void (Δ) will be left between the collapsed rock mass and main roof:

$$\Delta = M - (K_\rho - 1)\sum h \quad [5]$$

Equation [6] describes the sinkage of main roof.

$$s = \frac{L}{2}\sin\alpha - a\sin^2\alpha \approx \frac{L}{2}\sin\alpha \quad [6]$$

The magnitude of unfilled void (Δ) and main roof sinkage (s) can be compared to determine the style of main roof breakage. If $s > \Delta$ (Equations [7] and [8]), roof blocks are more likely to rotate, and blocks are supported by the collapsed rock mass before they fully detach.

$$s > \Delta \quad [7]$$

Equivalently:

$$\sum h > \frac{M - \frac{L}{2}\sin\alpha}{K_\rho - 1} \quad [8]$$

Accordingly, the roof is more likely to rotate and be classified in the fractured zone if the immediate roof thickness ($\sum h$) is larger; or mining height (M) is smaller; or the main roof first weighting/periodic distance (L) is larger; or the bulking factor (K_ρ) is larger.

Equations [9] and [10] show the main roof first and periodic weighting distances.

$$L = h\sqrt{\frac{2R_T}{q}} \quad [9]$$

$$L_0 = h\sqrt{\frac{R_T}{3q}} \quad [10]$$

where L and L_0 are the first and periodic roof weighting distance, respectively; R_T is main roof tensile strength; q is the vertical stress in the overlying strata (Qian and Shi, 2003). In other words, a thicker or stronger main roof or a shallower seam would lead to a larger first caving distance and hence involve the main roof in the fractured zone.

Physical modelling

Geomining conditions of Panel 8101

The representive physical simulation is based on Panel 8101 at Wangzhuang, which is worked by single-pass longwalling for the total extraction of a 6.3 m thick coal seam at 350–450 m depth. Panel 8101 inclines toward the southwest at an angle of 3°–7°. There are five interbedded dirt bands in the coal seam, with a total thickness of 0.78 m; the thickest band reaches 0.4 m thickness in part of the seam. The width of the longwall face is 270 m, and the length is 546 m.

Figure 4 depicts the general geological section of Wangzhuang coal mine. The 14.4 m immediate roof above the coal seam is weak, soft mudstone, and the 8.8 m main roof is fine-grained sandstone. The 5 m immediate floor and 2 m main floor are mudstone and fine-grained sandstone, respectively. The Protodikonov's Hardness Coefficient of the coal is 1.2. The coal type is excellent power coal, with low ash, sulphur, and phosphorus contents and a high calorific value.

Experimental solutions

Physical modelling is often used to visualize the behaviour of the overlying strata by simulating the field conditions in a model constructed from similar materials. In general, the most important similarities between the model mine and the actual mine should be adhered to if reliable results are to be obtained (Jiang *et al.*, 2011; Zhao *et al.*, 2013).

Geometric similarity:

The simulated equivalent material mine model was built on a 1:100 geomechanical scale. The ratio of model strata thickness to mine-scale strata thickness in the field is A_L=1/100.

$$A_L = \frac{L_m}{L_p}$$

where A_L is the geometric similarity ratio, and L_m and L_p are the thickness of model strata and full-scale strata, respectively

Time similarity:

$$A_T = \frac{T_m}{T_p} = \sqrt{A_L}$$

where A_T is the time similarity ratio, T_m and T_p are the mining time in the model and in field mining activity. A_T is 1/10 in this case.

Generalized Geological Section

Serial Number	Roofs and Floors	Layer Thickness (m)	Burial Depth	Scale 1:200	Rock Layer	Lithology
1	Main Roof	8.8	339.0		Fine-grain Sandstone	Dark gray, with slickenside and phytolite. Partly sandy mudstone at bottom.
2	Immediate Roof	14.4	353.4		Mudstone	Black, compact, with phytolite.
3	Coal #3	6.3	359.7		Coal	Excellent power coal, with 5 dirt bands (total thickness 0.78m).
4	Immediate Floor	5.0	364.7		Mudstone	Dark Gray, with phytolite.
5	Main Floor	2.0	366.7		Fine-grain Sandstone	Gray, mainly quartz feldspar, partly mudstone.

Figure 4 – General geological section

Unit weight similarity:

$$A_\gamma = \frac{\gamma_m}{\gamma_p}$$

where A_γ is the unit weight similarity ratio, and γ_m and γ_p are the unit weight of the model strata and field strata. Here A_γ is 1/1.7

Elasticity modulus and strength similarity:

$$A_E = A_\sigma = A_L A_\gamma$$

where A_E and A_σ (1/170) are elasticity modulus and strength similarity.

In this physical model, similar materials consist of aggregate (fine sand) and binders (gypsum, lime, and clay). The final physicomechanical properties depend on the proportions of these materials, hence, duplicate experiments were repeatedly conducted to obtain the correct proportions. Table II lists the material physicomechanical parameters of strata and the model dimension parameters.

The overall dimensions of the built model are 1 m × 1.2 m × 0.2 m. The model in Figure 5 shows the layout of the measuring points (small pins). Movements of these points were measured by an electronic theodolite and a digital camera before extraction, and were repeatly measured during every stage of extraction. The coal in the model is mined every 50 mm, which represents 5 m in mine scale.

Analysis of results

Coal is mined from right to left in the model. The dynamic movement of overlying strata was recorded by a digital camera during mining. An electronic theodolite was used to keep track of subsidence of strata. These photographs and data illustrate the movement of the overlying rock strata and roof caving and bending.

Roof caving characteristics

As the face advances, immediate roof caving initiates, followed by main roof bending, then periodic bending. Figure 6 illustrates this sequence of roof caving.

(1) Immediate roof caving

The immediate roof caves in during extraction due to low strength and the large unsupported area. An advance of the face to 25 m initiates the first small-scale caving of the immediate roof, 2 m in thickness (see Figure 6b). The first major fall occurs with a further 10 m advance (Figure 6c). The collapsed height in the overlying strata goes up to 21 m (starting from the bottom of the coal seam). These falling rocks are unable to fill the gob because of the large mining height.

(2) Main roof first bending

At 45 m of face advance, the limiting span of overhang of the main roof is met and the first roof weighting initiates (Figure 6d). Both rotation and sliding occur. The collapsed height reaches 32 m. A three-hinged arch is formed between the broken main roof blocks. The collapsed main roof blocks compact the falling immediate roof on the floor.

(3) Main roof periodic bending

After another 10 m of overhang, the main roof periodic weighting occurrs. Advance of the face to 55 m and 65 m generates periodic weighting (Figure 6e, 6f). The height of the affected roof strata extends up to around 36 m and 55 m, respectively. The three-hinged arch formed in the main roof supports the upper collapsed strata and compacts the lower falling rocks. It also can be seen that the separation between collapsed strata begins to close during face advance.

(4) Main roof last bending

After 80 m of face advance, the maximum height of the collapsed strata reaches nearly 70 m. The last periodic bending interval is 15 m. Overall, the height of collapsed strata increases gradually with face advance. The curve in Figure 7 shows this trend.

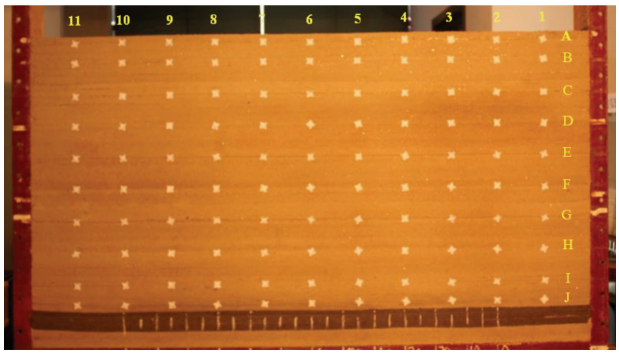

Figure 5 – Measuring points in the built model

Table II

Equivalent material physicomechanical parameters and model dimension parameters

Lithology	Strength MPa		Unit weight g/cm³		Cumulative thickness cm	Layer thickness cm	Layer weight kg	Sand weight kg	Lime weight kg	Paste weight kg	Water weight kg	Proportion
	Model	Field	Model	Field								
Mudstone	0.14	23	1.42	2.42	101.6	15	72.54	65.28	5.08	2.18	5.80	90:7:3
Mid-grain sandstone	0.38	65	1.53	2.6	86.6	14	67.20	58.80	4.20	4.20	5.38	70:5:5
Mudstone	0.14	23	1.42	2.42	72.6	15	72.54	65.28	5.08	2.18	5.80	90:7:3
Mid-grain sandstone	0.14	23	1.42	2.42	57.6	7.8	36.86	32.76	2.05	2.05	3.02	70:5:5
Fine-grain sandstone	0.34	58	1.65	2.8	49.8	4	19.30	17.16	1.07	1.07	1.54	80:5:5
Mid-grain sandstone	0.38	65	1.53	2.6	45.8	4.4	21.10	18.46	1.31	1.32	1.69	70:5:5
Mudstone	0.14	23	1.42	2.42	41.4	6.9	33.37	30.03	2.34	1.00	2.67	90:7:3
Fine-grain sandstone	0.34	58	1.65	2.8	34.5	8.8	42.40	37.68	2.36	2.36	3.39	80:5:5
Mudstone	0.14	23	1.42	2.42	25.7	14.4	69.60	62.64	4.87	2.09	5.57	90:7:3
Coal	0.07	12	0.79	1.35	11.3	6.3	30.53	27.75	2.22	0.56	2.44	100:8:2
Fine-grain sandstone	0.34	58	1.65	2.8	5	5	24.10	21.42	1.34	1.34	1.93	80:5:5

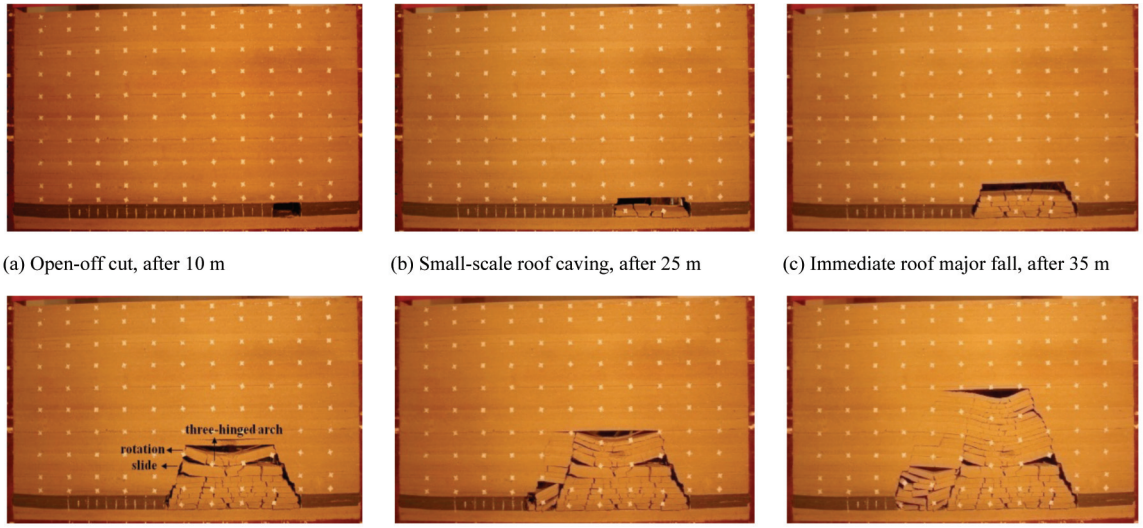

(a) Open-off cut, after 10 m (b) Small-scale roof caving, after 25 m (c) Immediate roof major fall, after 35 m

(d) Main roof first caving, after 45 m (e) Main roof second caving, after 55 m (f) Main roof third caving, after 65 m

Figure 6 – Model excavation roof caving sequence

After extraction of the face, three vertical zones and three horizontal areas can be distinguished, as shown in Figure 8. The broken small blocks from the immediate roof are deposited on the floor and are compacted by upper collapsed strata. The main roof is more likely to overhang for a larger distance and break into larger blocks, between which horizontal compressional forces are generated. The collapsed strata form a three-hinged arch shape due to the location of the supporting areas.

Overlying strata subsidence

The vertical displacement of the strata can be obtained by the changes in position of the measuring points, which are shown in Figure 9. As can be seen, the measuring points from the upper three measuring lines (A, B, and C, Figure 5) are almost coincident with the horizontal axis, which implies a displacement of almost zero. In contrast, the other strata (lines D to J) undergo significant subsidence, with both the amount of subsidence and the area affected by the subsidence increasing downward. The measurement points in row 5 indicate much greater subsidence than that in row 6, except for the two bottom lines (I and J) in the immediate roof. This is due mainly to the fact that points in row 5 are at the bottom of three-hinged arches. Lines I and J (located in immediate roof) are relatively steady, compared with significant fluctuations found from line E to H.

Fractured zone height

The bulking factor increases with decreasing rock strength (Xia *et al.*, 2014). The bulking factor is 1.1–1.2 if the roof is strong; 1.2–1.3 if the roof is medium strong; and 1.3–1.4 if the roof is weak. The main roof in Wangzhuang coal mine is medium-hard or weak. According to the model, main roof first bending distance (L) is 45 m. The mining thickness (M) is 6.3 m, and the bulking factor (K_ρ) is 1.2–1.4. Table III lists the calculated values of $(M–0.5\times L\times sin\alpha)/(K_\rho–1)$ (from Equation [8]) while the rotation angle (α) varies from 3° to 7° and the bulking factor (K_ρ) varies from 1.2 to 1.4.

To determine whether the main roof is included in the fractured or caved zone, it is necessary to compare the calculated values in Table III with the thickness of immediate roof ($\sum h$), or the thickness of strata that is potentially included in the caved zone. If Equation [8] is met, a roof of thickness of $\sum h$ is more likely to be incorporated in the fractured zone. If not, this roof is in caved zone.

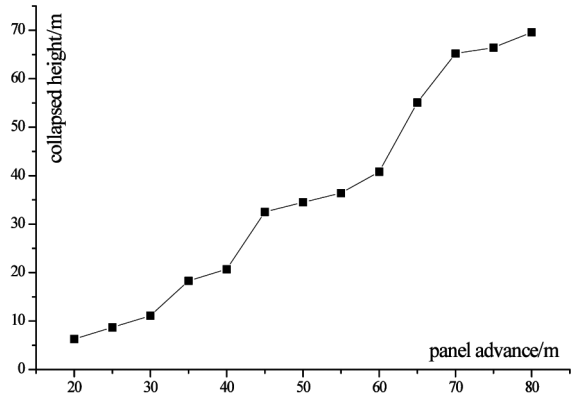

Figure 7 – Progressive collapsed height of roof strata

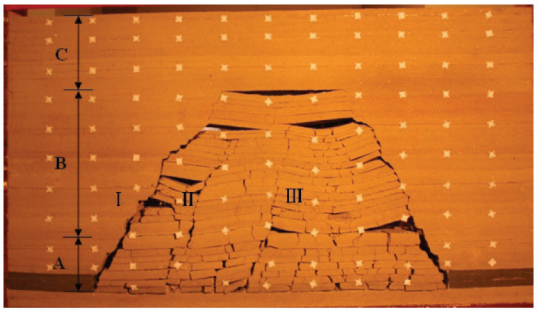

A -caved zone; B - fractured zone; C - continuous subsidence zone;

I- coal support area; II- separation area; III- recompactedarea

Figure 8 – The three vertical and three horizontal zones after extraction of the face

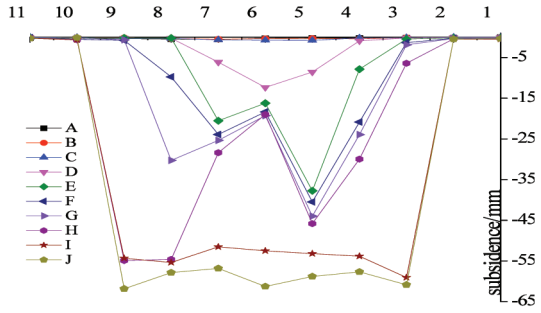

Figure 9 – Strata subsidence

During first main roof bending, $\sum h$=14.4<25.61 (α=3°, K_ρ=1.2, from Table III), so the immediate roof is included in the caved zone. In fact, it is obvious that no horizontal compressional force exists among immediate roof blocks in the model. The immediate roof is therefore assigned to the caved zone.

Then the roof of thickness of $\sum h$+0.5h is considered. Since $\sum h$+0.5h=18.8<20.49 (α=3°, K_ρ=1.25), lower main roof is also assigned to the caved zone. In the physical model, we can see that the lower main roof slides and no horizontal compressional force is generated, which verifies the theoretical solution.

Developing this method, $\sum h$+h=23.2>14.46 (α=5°, K_ρ=1.3), hence the upper roof is included in the fractured zone. It can be seen that upper main roof rotates and a three-hinged arch with horizontal compressional force between the blocks is generated (see Figure 10). The bottom of the upper main roof turns out to be the boundary of the caved and fractured zones.

During periodic main roof bending, the bending interval decreases to 10–15 m, but the bulking factor increases to 1.35 or more. As a result, the main roof is included in the fractured zone.

During the last main roof bending, the bending interval is 15 m, and falling immediate roof blocks are compacted (see Figure 8). It turns out that $\sum h$+h=23.2<59.07 (α=3°, K_ρ=1.1), so the main roof slides and roof blocks fail to generate compressional force. The main roof is included in the caved zone in this weighting.

To summarize, during first main roof weighting, the lower main roof is included in the caved zone but upper main roof is included in the fractured zone; in next two roof periodic weightings, the whole main roof is included in the fractured zone; but in the last main roof bending, the whole main roof is included in the caved zone. Thus the boundary between the caved and the fractured zones changes with face advance. In this study, it is believed that this boundary is the bottom of upper main roof (or top of lower main roof). The heights of the caved and fractured zones are given in Equations [11] and [12].

$$H_1 = K_\rho' \left(\sum h + \frac{1}{2} h \right) \quad [11]$$

$$H_2 = H_0 - H_1 \quad [12]$$

where K_ρ' (=1.1) is the ultimate bulking factor. H_0 (=69.6 m) is the collapsed height, H_1 is the caved zone height, and H_2 is the fractured zone height.

As a result, the calculated caved and fractured zone heights shown below are quite close to the results from empirical equations.

H_1=1.1×(14.4+4.4)=20.68 m

H_2=69.6-20.68=48.92 m

The continuous subsidence zone in this physical model is not actually subsiding, while subsidence of the ground surface in the field can be observed. However, the fractured and caved zones in this experiment are clear. The physical model can be improved in future research by, for instance, involving roof sag rates, exploring the influence of different key/competent strata (massive, strong strata above main roof), *etc.*

Roof fracture investigation

Boreholes were drilled into the roof in the transportation roadway of Panel 8101, and a borehole camera was used to record the fractures in the roof. Some fractures can be clearly seen (Figure 11).

Unfortunately the length of the boreholes is less than 7 m, thus the plotted fractures in the roof above the transportation roadway are from the caved zone. Photographs of fractures in the fractured zone could not be obtained. The fractures in different boreholes are mainly horizontal continuous fractures, and rather intensive, indicating that the fractures might be connecting by a horizontal fracture plane in the roof.

Conclusions

- Mining equipment, especially shields, enables annual production of high single-pass longwalling to increase to 14 Mt, the mining height to increase to 7 m, and recovery to increase to 96.7% in some longwalls in China. Further improvement in thick-seam coal mining will depend on innovation and the development of equipment
- The weak immediate roof is generally included in the caved zone. Breakage of the massive strong roof is classified into rotation and sliding, which determines whether the roof is included in the caved or fractured zone. Main roof sliding causes this roof to be

Table III

Calculated values

	K_ρ/α				
	1.2	**1.25**	**1.3**	**1.35**	**1.4**
3°	25.61	20.49	17.07	14.63	12.81
5°	21.69	17.36	14.46	12.40	10.84
7°	17.79	14.23	11.86	10.17	8.89

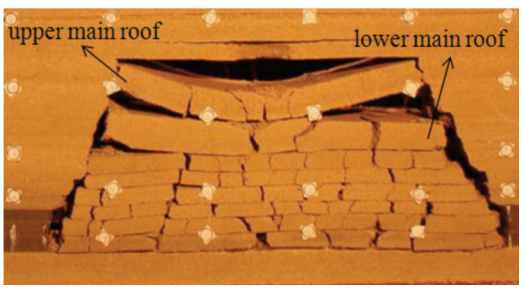

Figure 10 – Boundary between caved and fractured zones

incorporated in the caved zone, while main roof rotation incorporates it in the fractured zone, with horizontal forces generated between roof blocks
- A theoretical technique has been developed to determine the breakage mode of the roof, and thus the caved and fractured zone heights. The fractured zone height is closely related to mining height (M), immediate roof thickness ($\sum h$), bulking factor (K_ρ), main roof strength (R_T), main roof thickness (h), main roof weighting interval (L), and overlying strata stress (q). Of these, the bulking factor, mining height, and roof thickness are more relevant
- Representative physical modelling displays the three vertical zones and three horizontal areas. The collapsed height of the overlying strata is about 70 m. The main roof first weighting distance is 45 m, and the periodic weighting interval stands at 10–15 m. The maximum subsidence is 62 mm
- According to the analytical and physical models, the caved zone height is about 21 m and the fractured zone height is around 49 m, which is close to the results from the empirical equation.

Acknowledgements

The authors are grateful for Dr Sam Spearing's help. This paper is supported by The National Basic Research Program (973 Program, 2013CB227903), National Natural Science Foundation (U1361209), and CUMTB Research Fund for the Doctoral Program (00-800015z683).

References

Cui, X.M., Miao, X.X., Wang, J.A., Yang, S., Liu, H.D., Song, Y.Q., Liu, H., and Hu, X.K. 2000. Improved prediction of differential subsidence caused by underground mining. *International Journal of Rock Mechanics and Mining Sciences*, vol. 37. pp. 615–627.

Das, S.K. 2000. Observations and classification of roof strata behavior over longwall coal mining panels in India. *International Journal of Rock Mechanics and Mining Sciences*, vol. 37. pp. 585–597.

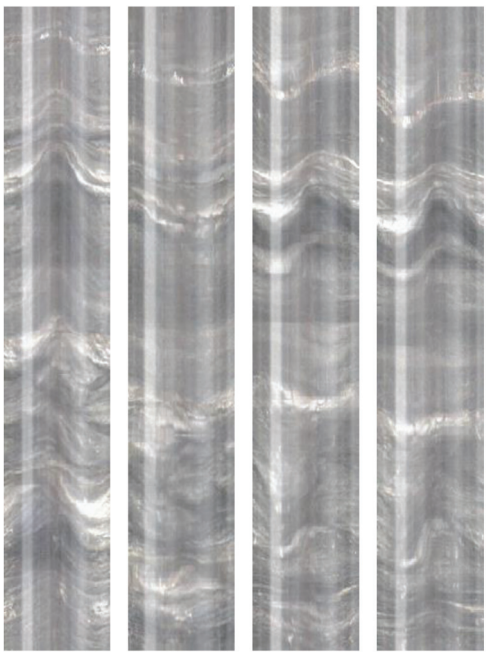

Figure 11 – Fractures in the roof

Hou, Z.J. 2003. The criterion on determining main roof in breaking zone and its application to the shallow seam. *Journal of China Coal Society*, vol. 28, no. 1. pp. 8–12 (in Chinese).

Hu, X.J., Li, W.P., Cao, D.T., and Liu, M.C. 2012. Index of multiple factors and expected height of fully mechanized water flowing fractured zone. *Journal of China Coal Society*, vol. 37, no. 4. pp. 613–620 (in Chinese).

Jiang, Y.D., Lv, Y.K., Zhao, Y.X., and Zhang, D.Y. 2011. Similar simulation test for breakage law of working face floor in coal mining above aquifer. *Chinese Journal of Rock Mechanics and Engineering*, vol. 30, no. 8. pp. 1571–1578 (in Chinese).

Ju, J.F. and Xu, J.L. 2013. Structural characteristics of key strata and strata behaviour of a fully mechanized longwall face with 7.0 m height chocks. *International Journal of Rock Mechanics and Mining Sciences*, vol. 58. pp. 46–54.

Kang, Y.H., Zhao, K.Q., Liu, Z.G., Tan, S.Y., Zhang, Y.J., Yi, D.L., Zhang, G.Y., and Li, L. 2009. Devastating laws of overlying strata with fissure under high hydraulic pressure. *Journal of China Coal Society*, vol. 34, no. 6. pp. 721–725 (in Chinese).

Li, X.Y., Li, J.P., Zhou, C.B., and Xiang, W.F. 2005. Comparative study on numerical simulation and similarity simulation of overburden deformation in abandoned stope. *Rock and Soil Mechanics*, vol. 26, no. 12. pp. 1907–1912 (in Chinese).

Qian, M.G. and Shi, P.W. 2003. Coal mine pressure and strata control. China University of Mining and Technology Press, Xuzhou (in Chinese).

Singh, R. and Singh, T.N. 1999. Investigation into the behaviour of a support system and roof strata during sublevel caving of a thick coal seam. *Geotechnical and Geological Engineering*, vol. 17. pp. 21–35.

State Bureau of Coal Industry. 2000. Regulations of buildings, water, railway and main well lane leaving coal pillar and press coal mining. China Coal Industry Publishing House, Beijing (in Chinese).

Sun, Q.X., Mu, Y., and Yang, X.L. 2013. Study on "two-zone" height of overlying of fully-mechanized technology with high mining thickness at Hongliu Coal Mine. *Journal of China Coal Society*, vol. 38, no. S2. pp. 283–286 (in Chinese).

Wagner, H. and Schümann, H.E.R. 1991. Surface effects of total coal-seam extraction by underground mining methods. *Journal of the South African Institute of Mining and Metallurgy*, vol. 91, no. 7. pp. 221–231.

Wang, G.F. 2013. Develop of fully-mechanized coal mining technology and equipment. *Coal Science and Technology*, vol. 41, no. 9. pp. 44–48 (in Chinese).

Wang, J.C. 2009. Theory and technology of thick seam mining. Metallurgical Industry Press, Beijing (in Chinese).

Wang, Z.Q., Li, P.F., Wang, L., Gao, Y., Guo, X.F., and Chen, C.F. 2013. Method of division and engineering use of "three band" in the stope again. *Journal of China Coal Society*, vol. 38, no. S2. pp. 287–293 (in Chinese).

Wu, R.X., Zhang, W., and Zhang, P.S. 2012. Exploration of parallel electrical technology for the dynamic variation of caving zone strata in coal face. *Journal of China Coal Society*, vol. 37, no. 4. pp. 571–577 (in Chinese).

Xia, X.G. and Huang, Q.X. 2014. Study on the dynamic height of caved zone based on porosity. *Journal of Mining and Safety Engineering*, vol. 31, no. 1. pp. 102–107 (in Chinese).

Xu, J.L., Wang, X.Z., Liu, W.T., and Wang, Z.G. 2009. Effects of primary key stratum location on height of water flowing fracture zone. *Chinese Journal of Rock Mechanics and Engineering*, vol. 28, no. 2. pp. 380–385 (in Chinese).

Xu, J.L., Zhu, W.B., and Wang, X.Z. 2012. New method to predict the height of fractured water-conducting zone by location of key strata. *Journal of China Coal Society*, vol. 37, no. 5. pp. 762–769 (in Chinese).

Yang, K., Xie, G.X., and Chang, J.C. 2009. Experimental investigation into mechanical characteristics of surrounding rock with different mining thickness. *Journal of China Coal Society*, vol. 34, no. 11. pp. 1446–1450 (in Chinese).

Yuan, Y., Tu, S.H., Wang, Y., Ma, X.T., and Wu, Q. 2010. Discussion on key problems and countermeasures of fully mechanized mining technology with high mining thickness. *Coal Science and Technology*, vol. 38, no. 1. pp. 4–8 (in Chinese).

Zhao, J.L. 2004. Research on new method of full-seam mining for gently inclined thick coal seams. China Coal Industry Publishing House, Beijing (in Chinese).

Zhao, Y.X., Jiang, Y.D., Lv, Y.K., and Cui, Z.J. 2013. Similar simulation experiment of bi-direction loading for floor destruction rules in coal mining above aquifer. *Journal of China Coal Society*, vol. 38, no. 3. pp. 384–390 (in Chinese). ◆